Laboratory Study of Magnetic Reconnection with a Density Asymmetry across the Current Sheet

Jongsoo Yoo,[1,*] Masaaki Yamada,[1] Hantao Ji,[1] Jonathan Jara-Almonte,[1] Clayton E. Myers,[1] and Li-Jen Chen[2]

[1]*Center for Magnetic Self-organization in Laboratory and Astrophysical Plasmas, Princeton Plasma Physics Laboratory, Princeton, New Jersey 08543, USA*

[2]*Space Science Center, University of New Hampshire, Durham, New Hampshire 03824, USA*

(Received 13 April 2014; published 28 August 2014)

The effects of a density asymmetry across the current sheet on anti-parallel magnetic reconnection are studied systematically in a laboratory plasma. Despite a significant density ratio of up to 10, the in-plane magnetic field profile is not significantly changed. On the other hand, the out-of-plane Hall magnetic field profile is considerably modified; it is almost bipolar in structure with the density asymmetry, as compared to quadrupolar in structure with the symmetric configuration. Moreover, the ion stagnation point is shifted to the low-density side, and the electrostatic potential profile also becomes asymmetric with a deeper potential well on the low-density side. Nonclassical bulk electron heating together with electromagnetic fluctuations in the lower hybrid frequency range is observed near the low-density-side separatrix. The dependence of the ion outflow and reconnection electric field on the density asymmetry is measured and compared with theoretical expectations. The measured ion outflow speeds are about 40% of the theoretical values.

DOI: 10.1103/PhysRevLett.113.095002 PACS numbers: 52.35.Vd, 52.30.-q

Magnetic reconnection is a fundamental process in magnetized plasmas which converts magnetic energy to particle energy. Magnetic reconnection plays a key role in explosive phenomena in the Universe such as geomagnetic storms, solar eruptions, and stellar flares [1–3]. Although the majority of theoretical and computational studies on magnetic reconnection assume that the plasma parameters on both sides of the current sheet are similar, magnetic reconnection often occurs with considerable asymmetries in upstream plasma parameters such as the plasma density and magnetic field strength [4–7]. For example, at the subsolar magnetopause, where the solar wind plasma interacts with the magnetospheric plasma, reconnection is mostly asymmetric with a large density ratio of 10–100 and a magnetic field strength ratio of 2–3. This so-called asymmetric reconnection is of importance due to its generality and applicability to real physical situations in both astrophysical plasmas [6] and magnetically confined laboratory plasmas [8,9].

Features of asymmetric reconnection have been observed in space [10,11] and numerical simulations [12–14]. In particular, the out-of-plane quadrupole magnetic field and the in-plane bipolar electric field, which are two signatures of collisionless reconnection, become almost bipolar and unipolar, respectively. Moreover, strong density gradients form near the low-density-side separatrix where strong electric field fluctuations are frequently observed [15,16]. The density asymmetry also impacts the ion flow pattern by shifting the ion inflow stagnation point to the low-density side [12,17].

The effects of asymmetrical upstream parameters on the reconnection rate and other exhaust-region properties, such as the density and outflow velocity, have been studied with a Sweet-Parker-type analysis [17]. Various 2D MHD simulations were performed to understand how the reconnection rate is determined during asymmetric reconnection [17–19]. Recently, the general scaling for asymmetric reconnection [17] has been tested in both two-fluid simulations [20,21] and particle-in-cell simulations [14].

Although there has been progress in understanding asymmetric reconnection, systematic experimental studies play an essential role in cross-validating observations in space and numerical simulations. In this Letter, the first quantitative analysis of asymmetric anti-parallel reconnection in a laboratory plasma is reported. Plasmas with a significant density ratio (up to 10) across the current sheet are created and compared with a nearly symmetric case with a density ratio of about 1.2. Key features of asymmetric reconnection, such as the modified Hall magnetic field and in-plane electrostatic potential, are experimentally verified. Furthermore, an asymmetric ion flow profile shows that the ion stagnation point is shifted to the low-density side. Strong bulk electron heating and electromagnetic fluctuations in the lower hybrid frequency range are observed near the low-density-side separatrix. Finally, both the ion outflow velocity and reconnection electric field are measured and compared with the general scaling laws in Ref. [17].

These experiments were performed at the Magnetic Reconnection Experiment (MRX) facility [22]. Figure 1(a) shows a cross section of the MRX device in the R–Z plane. The system is symmetrical along the toroidal (Y) direction. The two gray circles are "flux cores" that each contain two independent coils: a poloidal field (PF) coil and a toroidal

field (TF) coil. The PF coils produce the X-line magnetic field geometry, and reconnection is driven by decreasing the PF coil current [22]. The TF coils inductively create the plasma around the flux cores. No significant guide field exists during the quasisteady reconnection period over which the reconnection rate is relatively constant. The current sheet is elongated along the Z direction during the quasisteady period, such that the coordinate system in this Letter is the following: R is the normal to the current sheet; Z is the outflow direction; Y is the symmetric, out-of-plane direction. The plasma is in the collisionless regime, since the resistivity term balances less than 20% of the reconnection electric field at the X point [23].

In MRX, a density asymmetry is inherently generated during the plasma formation period due to the inductive electric field, E_{TF}, from the increasing TF coil current. For this experimental campaign, the direction of E_{TF} during the plasma formation is radially outward between the flux cores, as illustrated in Fig. 1(b). In this configuration, ions are transported radially outward along E_{TF}, generating a radial density asymmetry. After the plasma formation period, the radial density asymmetry decays over tens of Alfvén times. Thus, the density asymmetry during the quasisteady reconnection period depends on the TF current

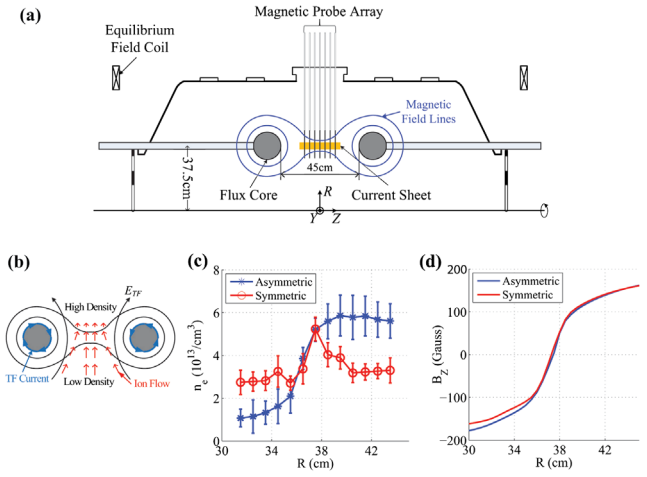

FIG. 1 (color online). (a) A cross section of MRX. The flux core contains both the PF coil for driving magnetic reconnection and the TF coil for creating the plasma. Magnetic probes are inserted to monitor the evolution of the 2D magnetic geometry. (b) Schematic view of the ion dynamics during the plasma formation period. The blue arrows along the flux cores indicate the direction of the TF coil current. The red arrows between the flux cores stand for the ion flow vectors. (c) Radial electron density profiles at $Z = 0$ for both asymmetric and symmetric cases early in the quasisteady period. The ion skin depth of the asymmetric case based on the low-density side is about 13 cm, while that of the symmetric case is 5 cm. (d) Radial profiles of the reconnecting magnetic field component (B_Z) at $Z = 0$ early in the quasisteady period. For the asymmetric case, the ion gyroradius is 5 cm, and the plasma β is about 0.14 on the low-density side. These quantities are not available for the symmetric case due to the lack of an ion temperature measurement in deuterium plasmas.

waveform, the gas species, and the fill pressure. In general, a plasma with more massive ions has a larger density asymmetry during the quasisteady period due to its longer Alfvén time. For example, we use helium to create an asymmetric plasma and deuterium to create a relatively symmetric plasma. In addition, the helium fill pressure is varied for further control of the density ratio up to 10.

The main diagnostic for this study is a 2D magnetic probe array which consists of 250 small pick-up coils. The probe array measures the evolution of all three components of the magnetic field with a maximum radial (R) resolution of 0.6 cm and an axial (Z) spacing of 3 cm. The electron density (n_e) and temperature (T_e) are measured by triple Langmuir probes [24]. The plasma potential (Φ_p) is obtained by measuring floating potential and electron temperature profiles [25]. The ion flow vectors ($\mathbf{V}_i$) are measured by Mach probes which were previously calibrated by spectroscopic data [25]. A fluctuation probe is used to measure all three components of magnetic fluctuations and the out-of-plane (Y) component of electrostatic fluctuations in the floating potential. Extensive R-Z scans of Langmuir probes and Mach probes are conducted to obtain 2D profiles of n_e, T_e, Φ_p, and $\mathbf{V}_i$ for both asymmetric (4.5 mT helium discharges) and symmetric (4 mT deuterium discharges) cases. In each case, about 2400 discharges are scrutinized for reproducibility based on both the data from the 2D magnetic probe array and a reference Langmuir probe. About 35% of discharges are used to produce data presented in this Letter.

Figure 1(c) shows clear differences in the radial density profile at $Z = 0$ between the asymmetric and symmetric case early in the quasisteady period. For the asymmetric case, the outboard side ($R > 37.5$ cm) has about 6 times more density than the inboard side ($R < 37.5$ cm). It is worth noting that a strong density slope appears on the low-density side ($R < 37.5$ cm). In fact, the measured 2D density profile (not shown) shows that strong density gradients occur in the vicinity of the low-density-side separatrix throughout the downstream region, which is consistent with numerical simulations [12–14] and space observations (e.g., [26]). For the symmetric case, the upstream densities are very similar, and the density peaks at the center of the current sheet ($R = 37.5$ cm).

In contrast to the density profiles, the reconnecting magnetic field (B_Z) profiles at $Z = 0$ are remarkably similar for both cases, as shown in Fig. 1(d). Despite the large density asymmetry, the low-density side has only about 15% larger B_Z magnitude than the high-density side. The magnetic pressure difference between the two sides of the current sheet is only about 15 Pa, which is not enough to enforce pressure balance across the current sheet if the electron and ion temperature on each side are similar. Thus, electron and ion temperature are expected to be higher on the low-density side. The T_e profile is indeed asymmetric [see Fig. 4(a)] with higher temperatures on the low-density side, but the pressure increase from the high electron temperature is about 4 Pa,

which is not enough to ensure pressure balance. This indicates that the ion temperature on the low-density side should also be higher. Because of the lack of ion temperature measurements with high radial resolution, however, this expectation has not been confirmed. Another possible explanation is the transient nature of the MRX discharge. Both the density asymmetry and ion flow pattern change on a time scale that is slower than the local Alfvén time during the quasisteady reconnection period.

As shown in Figs. 2(a) and 2(b), there is no noticeable difference in the in-plane magnetic geometry between the two cases. The in-plane magnetic geometry is presented with the black lines, which are contours of the poloidal magnetic flux, $\Psi \equiv \int_0^R 2\pi R' B_Z dR'$. Assuming a toroidal symmetry, these contours represent the magnetic field lines in the R-Z plane.

While the density asymmetry does not affect the in-plane magnetic geometry, it significantly modifies the Hall magnetic field profile, as shown with the color in Figs. 2(a) and 2(b). The Hall magnetic field profile for the asymmetric case is significantly different from that of the symmetric case; the magnitude of the Hall magnetic field is about 6 times larger on the high-density side than on the low-density side.

This asymmetric Hall magnetic field profile can be explained by the Hall term in the generalized Ohm's law. The reconnection electric field ($E_{\rm rec}$) is relatively uniform on both sides during the quasisteady reconnection period, and it is balanced by the $\mathbf{J} \times \mathbf{B}$ Hall term in the upstream region [27]. Thus, we have

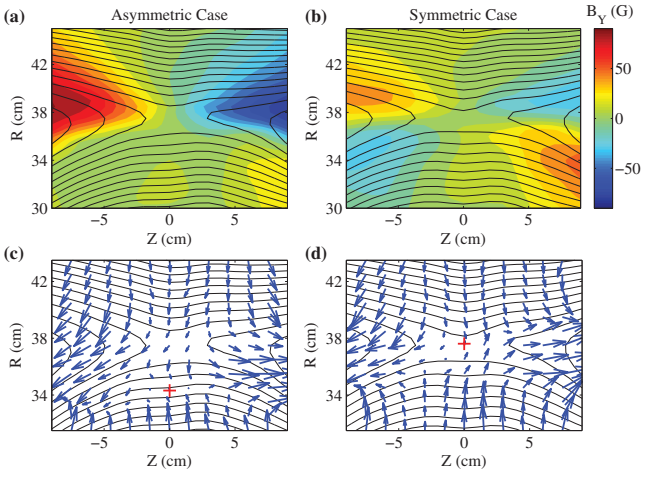

FIG. 2 (color). 2D profiles of the out-of-plane magnetic field (B_Y) with contours of the poloidal flux for asymmetric (a) and symmetric (b) cases. Compared to the symmetric case, the Hall magnetic field component is enhanced on the high-density side ($R > 37.5$ cm) and suppressed on the low-density side ($R < 37.5$ cm). Black lines indicate contours of the poloidal magnetic flux which represent magnetic field lines. In-plane ion flow vector profiles for asymmetric (c) and symmetric (d) cases. Red crosses indicate the radial location of $V_R = 0$ at $Z = 0$. For the asymmetric case, the ion inflow stagnation point is shifted to the low-density side. The density ratio (n_1/n_2) for the asymmetric case is about 6, while it is about 1.2 for the symmetric case.

$$E_{\rm rec} \approx -\frac{J_1 B_1}{e n_1} \approx -\frac{J_2 B_2}{e n_2}, \quad (1)$$

where subscript 1 indicates upstream quantities on the high-density side, while the subscript 2 means those on the low-density side. From this equation, the Hall current of the high-density side, $J_1 \approx (n_1 B_2)/(n_2 B_1) J_2 \approx (n_1/n_2) J_2$ is larger by about the density ratio. Since the Hall magnetic field is generated by the Hall current, the high-density side has a larger magnitude.

The in-plane ion flow pattern is affected by the density asymmetry as shown in Figs. 2(c) and 2(d). The red crosses indicate the location of $V_R = 0$ at $Z = 0$. For the asymmetric case, the inflow ion stagnation point is shifted to $R \sim 34.5$ cm, while the X point is at 37.5 cm. For the symmetric case, the stagnation point at $Z = 0$ is almost at the same location as the X point. This shift of stagnation point is due to the imbalance of the incoming mass flux [17] and is observed in numerical simulations [12]. It is worth noting that the ion outflow is also asymmetric, especially on the left side ($Z = 7.5$ cm); the ion outflow is stronger on the low-density side that has a larger upstream Alfvén velocity [19].

The density asymmetry also modifies the in-plane electrostatic potential profile, which is another signature of collisionless reconnection. The in-plane electrostatic potential has a "well" structure along the direction normal to the current sheet [25,28–30]. Figure 3 shows radial potential profiles at $Z = 0$ for both asymmetric and symmetric cases. The depth of the potential well on the low-density side is about 3–4 times larger than that on the low-density side. For the symmetric case, the potential profile is balanced with a well depth of about 9 V. This modified potential profile is expected since the depth of the potential well scales as B^2/n_e [23].

Figure 4(a) shows the measured 2D electron temperature profile. Electrons are strongly heated near the low-density-side separatrix where fluctuations in both E_Y and $\mathbf{B}$ are

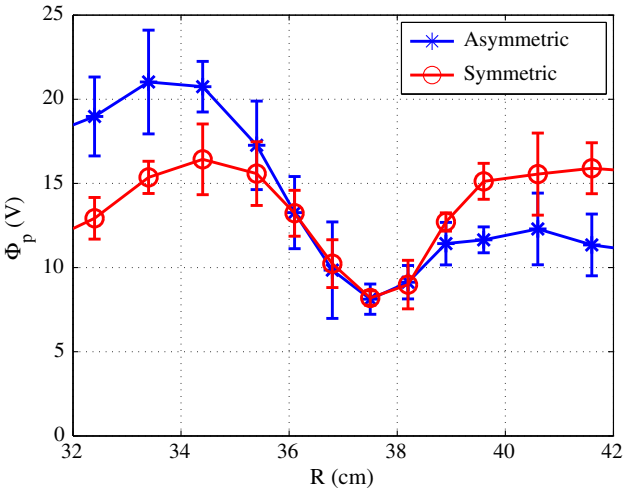

FIG. 3 (color online). Radial plasma potential profiles at $Z = 0$ for asymmetric (blue) and symmetric (red) cases. With the density asymmetry, the potential profile becomes asymmetric with a larger well depth on the low-density side.

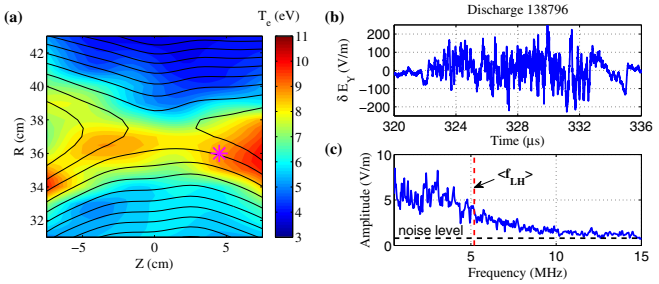

FIG. 4 (color online). (a) 2D electron temperature profile for the asymmetric case. Strong bulk electron heating exists near the low-density-side separatrix. The magenta asterisk indicates the measurement location of high-frequency fluctuations. (b) Time trace of typical fluctuations in E_Y (Discharge 138 796). (c) Fourier spectrum of δE_Y averaged over 12 discharges.

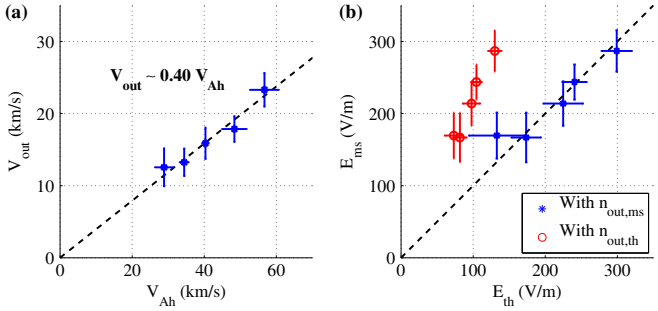

FIG. 5 (color online). (a) Measured ion outflow velocity compared to the hybrid Alfvén velocity. The measured values are about 40% of theoretically predicted values. The black dashed line indicates a linear fit. (b) The measured reconnection electric field versus $E_{\rm th}$ in Eq. (3). Values of $E_{\rm ms}$ agree with those of $E_{\rm th}$ when the measured outflow density, $n_{\rm out,ms}$ (blue asterisks) is used as $n_{\rm out}$ instead of the theoretical estimate, $n_{\rm out,th}$ (red circles).

observed. A 2D heat transport analysis reveals that the observed electron heating is beyond classical Ohmic dissipation based on the Spitzer resistivity, which is consistent with the previous measurements during quasi-symmetric reconnection [23,32]. Figure 4(b) shows a time trace of fluctuations in the out-of-plane electric field (δE_Y). The trace of fluctuations in the magnetic field is similar, and typical amplitudes of δE_Y and δB are 100 V/m and 7 Gauss, respectively. The averaged Fourier spectrum in Fig. 4(c) shows that these fluctuations are broadband and that the energy is mostly concentrated below the lower-hybrid (LH) frequency, $f_{\rm LH}$. These characteristics are consistent with lower-hybrid drift instability (LHDI) driven turbulence [15,16,31–34]. The free energy source of LHDI is the strong density gradient in the vicinity of the low-density-side separatrix [15]. This LHDI driven turbulence may contribute to the observed bulk electron heating [33]. However, the effective electron heating by the parallel electric field can also play a role [35]. The parallel electric field in the asymmetric configuration exists only on the low-density side [35]. The measured 2D profile supports the existence of the parallel electric field, since the upstream temperature on the low-density side (~6 eV) is higher than the high-density side (~4 eV). More detailed measurements and analyses are required to identify the dominant mechanism(s) for the observed electron heating.

Finally, the general scaling for the ion outflow and reconnection electric field given by Ref. [17] is tested by systematically varying the density ratio (n_1/n_2). Plasmas with different $n_1 = (1.3\text{–}10) \times 10^{13}/\text{cm}^3$ and relatively constant $n_2 \sim 1 \times 10^{13}/\text{cm}^3$ are created. The ion outflow is measured about $1.5d_i$ away from the X point where $d_i \equiv c/\omega_{pi}$ is the ion skin depth based on n_2. The radial location of the measurement is $R = 37.5$ cm. As shown in Fig. 5(a), the measured outflow velocity $V_{\rm out}$ is only 40% of the theoretically predicted outflow velocity $V_{\rm Ah}$. Here, $V_{\rm Ah}$ is a hybrid Alfvén velocity defined as [17]

$$m_i V_{\rm Ah}^2 = \frac{S_1 + S_2}{n_1 V_1 + n_2 V_2} = \frac{B_1 B_2 (B_1 + B_2)}{\mu_0 (n_1 B_2 + n_2 B_1)}, \qquad (2)$$

where S_1 and S_2 are the incoming Poynting fluxes and V_1 and V_2 are the inflow speeds. Since $m_i V_{\rm Ah}^2$ is the ratio of incoming Poynting fluxes and particle fluxes, it physically represents the available magnetic energy per an ion-electron pair [36]. Therefore, for the plasma to have the outflow speed of $V_{\rm Ah}$, about one half of the available magnetic energy would have to be converted to the ion flow energy. However, the energy inventory during magnetic reconnection generally favors increasing the ion thermal energy rather than flow energy [19,37–39]. In MRX, there is another possible reason for the low outflow velocity, which is the high downstream pressure due to the presence of the flux cores [25,40].

The measured reconnection electric field ($E_{\rm ms}$) is also compared to the theoretical prediction ($E_{\rm th}$), which is given by [17]

$$E_{\rm th} = \frac{2\delta}{L} V_{\rm out} \frac{n_{\rm out} B_1 B_2}{n_1 B_2 + n_2 B_1}, \qquad (3)$$

where δ and L are the half width and length of the diffusion region, respectively, and $n_{\rm out}$ is the density at the outflow region. By arguing $n_{\rm out}$ is the effective density of a newly reconnected flux tube, the theoretical estimate of $n_{\rm out}$ is given by [17]

$$n_{\rm out,th} = \frac{B_1 n_2 + B_2 n_1}{B_1 + B_2}. \qquad (4)$$

However, the measured density at the outflow region, $n_{\rm out,ms}$ is about $2n_{\rm out,th}$. This higher measured $n_{\rm out}$ may come from the back pressure due to the flux cores. As shown in Fig. 5(b), $E_{\rm ms}$ agrees with $E_{\rm th}$ only if we use the measured outflow density as $n_{\rm out}$ in Eq. (3).

In summary, we have studied reconnection with a significant density asymmetry in a laboratory plasma. The observed features of asymmetric reconnection agree with previous observations in space and numerical simulations. The density asymmetry modifies the in-plane ion flow pattern as well as the Hall fields—the quadrupole

out-of-plane magnetic field and in-plane electrostatic field. However, the in-plane magnetic field geometry is barely affected. Strong bulk electron heating is observed near the low-density-side separatrix together with electromagnetic fluctuations driven by LHDI. Mechanisms for the electron heating require further research. The ion outflow and reconnection electric field are measured and compared with theoretical predictions. The ion outflow speed is about 40% of the hybrid Alfvén velocity and the reconnection electric field agrees with the scaling, provided that the measured plasma density in the exhaust region is used instead of the theoretically predicted value. In the future, direct comparisons between laboratory data and spacecraft data at the subsolar magnetopause will be attempted for more understanding of particle energization during asymmetric reconnection.

This work is supported by CMSO, DOE Contract No. DE-AC0209CH11466, the NASA program for the MMS mission under the Grant No. NNH11AQ45I, and the NSF Grant No. AGS-1202537. The authors thank J. Drake, V. Roytershteyn, M. Shay, and W. Daughton for valuable discussions, and R. Cutler for technical support.

*jyoo@pppl.gov

[1] E. Priest and T. Forbes, *Magnetic Reconnection: MHD Theory and Applications* (Cambridge University Press, New York, 2000).
[2] E. G. Zweibel and M. Yamada, Annu. Rev. Astron. Astrophys. **47**, 291 (2009).
[3] M. Yamada, R. Kulsrud, and H. Ji, Rev. Mod. Phys. **82**, 603 (2010).
[4] M. Øieroset, T. D. Phan, and M. Fujimoto, Geophys. Res. Lett. **31**, L12801 (2004).
[5] F. S. Mozer and A. Retinò, J. Geophys. Res. **112**, A10206 (2007).
[6] F. S. Mozer and P. L. Pritchett, Space Sci. Rev. **158**, 119 (2011).
[7] J. P. Eastwood, T. D. Phan, M. ieroset, M. A. Shay, K. Malakit, M. Swisdak, J. F. Drake, and A. Masters, Plasma Phys. Controlled Fusion **55**, 124001 (2013).
[8] L. Zakharov, B. Rogers, and S. Migliuolo, Phys. Fluids B **5**, 2498 (1993).
[9] M. T. Beidler and P. A. Cassak, Phys. Rev. Lett. **107**, 255002 (2011).
[10] F. S. Mozer, V. Angelopoulos, J. Bonnell, K. H. Glassmeier, and J. P. McFadden, Geophys. Res. Lett. **35**, L17S04 (2008).
[11] F. S. Mozer, P. L. Pritchett, J. Bonnell, D. Sundkvist, and M. T. Chang, J. Geophys. Res. **113**, A00C03 (2008).
[12] P. L. Pritchett, J. Geophys. Res. **113**, A06210 (2008).
[13] K. G. Tanaka, A. Retinò, Y. Asano, M. Fujimoto, I. Shinohara, A. Vaivads, Y. Khotyaintsev, M. André, M. B. Bavassano-Cattaneo, S. C. Buchert, and C. J. Owen, Ann. Geophys. **26**, 2471 (2008).
[14] K. Malakit, M. A. Shay, P. A. Cassak, and C. Bard, J. Geophys. Res. **115**, A10223 (2010).
[15] P. L. Pritchett, F. S. Mozer, and M. Wilber, J. Geophys. Res. **117**, A06212 (2012).
[16] V. Roytershteyn, W. Daughton, H. Karimabadi, and F. S. Mozer, Phys. Rev. Lett. **108**, 185001 (2012).
[17] P. A. Cassak and M. A. Shay, Phys. Plasmas **14**, 102114 (2007).
[18] J. E. Borovsky and M. Hesse, Phys. Plasmas **14**, 102309 (2007).
[19] J. Birn, J. E. Borovsky, and M. Hesse, Phys. Plasmas **15**, 032101 (2008).
[20] P. A. Cassak and M. A. Shay, Geophys. Res. Lett. **35**, L19102 (2008).
[21] P. A. Cassak and M. A. Shay, Phys. Plasmas **16**, 055704 (2009).
[22] M. Yamada, H. Ji, S. Hsu, T. Carter, R. Kulsrud, N. Bretz, F. Jobes, Y. Ono, and F. Perkins, Phys. Plasmas **4**, 1936 (1997).
[23] J. Yoo, M. Yamada, H. Ji, J. Jara-Almonte, and C. E. Myers, Phys. Plasmas **21**, 055706 (2014).
[24] S.-L. Chen and T. Sekiguchi, J. Appl. Phys. **36**, 2363 (1965).
[25] J. Yoo, M. Yamada, H. Ji, and C. E. Myers, Phys. Rev. Lett. **110**, 215007 (2013).
[26] Y. V. Khotyaintsev, A. Vaivads, A. Retinò, M. André, C. J. Owen, and H. Nilsson, Phys. Rev. Lett. **97**, 205003 (2006).
[27] Y. Ren, M. Yamada, H. Ji, S. Dorfman, S. P. Gerhardt, and R. Kulsrud, Phys. Plasmas **15**, 082113 (2008).
[28] J. R. Wygant, C. A. Carttell, R. Lysak, Y. Song, J. Dombeck, J. McFadden, F. S. Mozer, C. W. Carlson, G. Parks, E. A. Lucek, A. Balogh, M. Andre, H. Reme, M. Hesse, and C. Mouikis, J. Geophys. Res. **110**, A09206 (2005).
[29] H. Karimabadi, W. Daughton, and J. Scudder, Geophys. Res. Lett. **34**, L13104 (2007).
[30] L.-J. Chen, N. Bessho, B. Lefebvre, H. Vaith, A. Fazakerley, A. Bhattacharjee, P. A. Puhl-Quinn, A. Runov, Y. Khotyaintsev, A. Vaivads, E. Georgescu, and R. Torbert, J. Geophys. Res. **113**, A12213 (2008).
[31] T. A. Carter, H. Ji, F. Trintchouk, M. Yamada, and R. M. Kulsrud, Phys. Rev. Lett. **88**, 015001 (2001).
[32] H. Ji, S. Terry, M. Yamada, R. Kulsrud, A. Kuritsyn, and Y. Ren, Phys. Rev. Lett. **92**, 115001 (2004).
[33] X. Tang, C. Cattell, J. Dombeck, L. Dai, L. B. Wilson, A. Breneman, and A. Hupach, Geophys. Res. Lett. **40**, 2884 (2013).
[34] V. Roytershteyn, S. Dorfman, W. Daughton, H. Ji, M. Yamada, and H. Karimabadi, Phys. Plasmas **20**, 061212 (2013).
[35] J. Egedal, A. Le, P. L. Pritchett, and W. Daughton, Phys. Plasmas **18**, 102901 (2011).
[36] T. D. Phan, M. A. Shay, J. T. Gosling, M. Fujimoto, J. F. Drake, G. Paschmann, M. Oieroset, J. P. Eastwood, and V. Angelopoulos, Geophys. Res. Lett. **40**, 4475 (2013).
[37] N. Aunai, G. Belmont, and R. Smets, Phys. Plasmas **18**, 122901 (2011).
[38] J. P. Eastwood, T. D. Phan, J. F. Drake, M. A. Shay, A. L. Borg, B. Lavraud, and M. G. G. T. Taylor, Phys. Rev. Lett. **110**, 225001 (2013).
[39] M. Yamada, J. Yoo, J. Jara-Almonte, H. Ji, R. M. Kulsrud, and C. E. Myers (to be published).
[40] H. Ji, M. Yamada, S. Hsu, and R. Kulsrud, Phys. Rev. Lett. **80**, 3256 (1998).